arXiv:1410.4577v1 [cond-mat.soft] 16 Oct 2014

Intra-Globular Structures in Multiblock Copolymer Chains from a Monte Carlo Simulation

K. Lewandowski[1] and M. Banaszak[1,*]

[1] *Faculty of Physics, A. Mickiewicz University*

ul. Umultowska 85, 61-614 Poznan, Poland

(Dated: October 20, 2014)

Abstract

Multiblock copolymer chains in implicit nonselective solvents are studied by Monte Carlo method which employs a parallel tempering algorithm. Chains consisting of 120 A and 120 B monomers, arranged in three distinct microarchitectures: $(10{-}10)_{12}$, $(6{-}6)_{20}$, and $(3{-}3)_{40}$, collapse to globular states upon cooling, as expected. By varying both the reduced temperature T^* and compatibility between monomers ω, numerous intra-globular structures are obtained: diclusters (handshake, spiral, torus with a core, etc.), triclusters, and n-clusters with $n > 3$ (lamellar and other), which are reminiscent of the block copolymer nanophases for spherically confined geometries. Phase diagrams for various chains in the (T^*, ω)-space are mapped. The structure factor $S(k)$, for a selected microarchitecture and ω, is calculated. Since $S(k)$ can be measured in scattering experiments, it can be used to relate simulation results to an experiment. Self-assembly in those systems is interpreted in term of competition between minimization of the interfacial area separating different types of monomers and minimization of contacts between chain and solvent. Finally, the relevance of this model to the protein folding is addressed.

* mbanasz@amu.edu.pl; http://www.simgroup.amu.edu.pl

I. INTRODUCTION

A single multiblock copolymer chain in a nonselective solvent is an interesting system to study because of its potential to form various nanostructures in a globular state, such as: double droplet, lamellar, hand shake, spiral, and disordered globule[1]. Those nanostructures are reminiscent of phases observed in block copolymer melts[2, 3], in general, and in confined geometries[4–9], in particular. Confinement can be one dimensional (thin films)[4], two dimensional (cylindrical pores)[5–7], and three dimensional (spherical pores)[8, 9]. The latter is the most relevant analogue for a single polymer chain in a poor solvent, since the chain collapses and tends to form a spherical globule. Copolymer chains in spherical confinement, with the interaction parameters similar to those considered in this work, were studied, using a coarse-grained model, in reference 8. The following structures, corresponding to those identified in multiblock copolymer chains, were identified[8]: spheres with layers, helical-like or handshake-like structures, and tricluster structures.

Ordering of copolymer nanostructures is driven by both lowering the temperature, which results in decreasing the solvent quality, and lowering the compatibility between A and B, leading to a coil-to-globule transition and a subsequent segregation of A and B monomers within the globule. There are interesting analogies:

- the formation of a globule is a condensation of monomers, which is similar to a gas-liquid transition,
- segregation of A and B monomers resembles disorder-order and order-order transitions, resulting in structures similar to those of copolymers in confined geometries.

At considerably lower temperatures the polymer chains crystallize, undergoing both liquid-solid and solid-solid transitions, with interesting packing effects, as shown recently for homopolymers [10–12].

An additional motivation for this study is its possible relation to structural transformations in biopolymers[13]. For example, the simplest models of proteins also employ only two types of building blocks that is hydrophilic, also referred to as polar (P), and hydrophobic (H) [14, 15]. These models, despite their excessive simplicity, provide basic insight into formation of secondary and tertiary structures, but in comparison to models with more types of monomers, they result in less cooperative folding and also in less designing sequences[13, 16–

18]. The sequence is referred to as designing when it can fold to the unique native state, that is the ground state with the lowest energy.

Majority of sequences in the HP model lead to degenerate native states, unlike most proteins which exhibit the native state with fluctuations which probe various conformational sub-states. Those sub-states are often very close to the native state, and are caused by thermal fluctuations of atoms and slight displacements of amino acids [19]. Increasing the number of types of monomers, with various interaction energies (for example, as calculated in Ref. 20), can improve these models in terms of reproducing the properties of the real protein systems[21]. A modification of the HP model, such as a change of the interaction energy between H and P monomers, can also improve this model noticeably [18]. In this work, we also use only two types of monomers, A and B, but in nonselective solvent, and this can provide some insight into ordering of proteins with hydrophobic amino acids within the hydrophobic core. It is worthwhile to reiterate that both monomers mimick the hydrophobic behavior, at low temperatures, since the solvent is nonselective.

The specific goals of the study are as follows:

- to identify intra-globular structures of long multiblock copolymer chains with different compatibilities,
- to construct phase diagrams for those structures,
- to calculate structure factors for selected chains,
- to relate results to protein folding problem.

II. MODEL

A. Simulation box and environment

Simulation is performed in a cubic box and the usual periodic boundary conditions are imposed. The simulation box size is sufficiently large for a chain to fit in, and not to interact with itself across boundary conditions. We simulate a single polymer chain and polymer-solvent interactions are included in an implicit manner in polymer-polymer interaction potential[22]. This can be considered as a dilute polymer solution.

B. Polymer model

We use a coarse-grained model for the polymer chain with monomers of diameter σ, taken also as the length unit. In this work, by "monomer" we mean the basic building unit of the coarse-grained chain. Monomers are of two types: A and B. Neighboring monomers along the chain are connected via the bond potential:

$$U_B(r) = \begin{cases} \infty & \text{for } r < \sigma \\ 0 & \text{for } \sigma \leq r \leq \sigma + \eta \\ \infty & \text{for } r > \sigma + \eta \end{cases} \tag{1}$$

where $\sigma + \eta$ is the maximum bond length, and $\sigma + \frac{1}{2}\eta$ is considered to be the average bond length.

Monomers that are not adjacent along the chain (nonbonded monomers), interact via the following square well potential:

$$U_N(r) = \begin{cases} \infty & \text{for } r < \sigma \\ \epsilon_{ij} & \text{for } \sigma \leq r \leq \sigma + \mu \\ 0 & \text{for } r > \sigma + \mu \end{cases} \tag{2}$$

where $\sigma + \mu$ is range of the interaction potential, ϵ_{ij} is interaction energy between monomers of types i and j. We assume that $\mu = \frac{1}{4}\sigma$, and $\eta = \frac{1}{4}\sigma$[23].

Chain bonds are not allowed to be broken, however they are allowed to be stretched. Interaction parameter ϵ_{ij} is defined as:

$$\begin{aligned} \epsilon_{AA} = \epsilon_{BB} = -\epsilon \\ \epsilon_{AB} \in [-\epsilon; -0.1\epsilon] \end{aligned} \tag{3}$$

The ϵ parameter, which is positive, serves as an energy unit to define the reduced energy per monomer E^*/N, and the reduced temperature T^* as:

$$\begin{aligned} E^*/N = \left(\tfrac{E}{\epsilon}\right)/N, \\ T^* = k_B T/\epsilon \end{aligned} \tag{4}$$

where N is the number of chain monomers, and k_B is Boltzmann constant. Negative ϵ_{ij}'s indicate that there is an attraction between monomers, and the presence of the solvent is taken into account in an implicit manner[22]. By controlling the relative strength of this

attraction, via T^*, we effectively vary solvent quality, from good to bad, which causes a collapse of the polymer chain, from a swollen state to a globular state[23–25]. The swollen and collapsed states are separated by the Θ solvent state, where the chain is Gaussian. This state is characterized by a temperature T^*_Θ, which is of the order of unity $T^*_\Theta \sim 1$ for this model. Since we are interested in intra-globular structures, we mostly concentrate on temperatures below the Θ-temperature.

Because we vary ϵ_{AB}'s in this work, a dimensionless parameter, $\omega = -\epsilon_{AB}/\epsilon$ is introduced, which is a measure of compatibility between A and B monomers. Lower values of ω mean lower compatibility. As we increase ω from 0.1 to 1, we make the monomers increasingly compatible, and for $\omega = 1$ they become identical, converting the copolymer chain into the homopolymer chain.

C. Polymer architecture

While we use only one chain length $N = 240$, with 120 A monomers and 120 B monomers, different multiblock microarchitectures are considered: $(10-10)_{12}$, $(6-6)_{20}$, and $(3-3)_{40}$. For the largest block size, $(10-10)_{12}$, the A and B monomers are expected to separate more easily at low temperatures, but for smaller block sizes it may be more difficult to separate them into two phases because of geometric frustrations.

D. Cluster count distribution

We differentiate between intra-globular structures by the number of clusters of A and B monomers, and also by the shape of those clusters. We define cluster as a group of monomers of the same type that are connected with each other either, directly or via a connected path of monomers, and two monomers are connected if their distance is smaller than the range of interaction potential. We count the clusters in simulation, and determine the equilibrium cluster count distribution (CCD) which is the probability distribution for different counts of clusters.

For each chain architecture and ω, CCD is calculated and plotted as a function of T^*. These plots are used to determine the phase diagrams in the (T^*, ω)-space for each microarchitecture. Since n-clusters, with different n, can coexist for a given (T^*, ω), we show only

the most probable structures in phase diagrams.

III. METHOD

We use the Metropolis[26] acceptance criteria for the Monte Carlo (MC) moves. The MC moves are chain rotations, translations, crankshaft rotations, and slithering snake moves. A Monte Carlo step (MCS) is defined as an attempt to move once each monomer of the chain.

Moreover, we use parallel tempering (replica exchange) Monte Carlo[27] (PT) with feedback-optimized parallel tempering method[28, 29] (FOPT). In the PT method M replicas of system are simulated in parallel, each at a different temperature T_i^*, with i ranging from 1 to M. After a number of MCS (in this work it is 100 MCS) we try to exchange replicas with neighboring T_i^* in random order with probability:

$$p(T_i^* \leftrightarrow T_{i+1}^*) = \min[1, \exp(-(\beta_i - \beta_{i+1})(U_{i+1} - U_i))] \tag{5}$$

where $\beta_i = 1/k_B T_i^*$ and U_i is potential energy of replica at T_i^*.

Correctly adjusted PT method allows a better probing of the phase space of the system and prevents trapping in energy minima at low temperatures. Thus it allows us to obtain better statistics in simulation and after a single simulation we obtain results for the selected range of temperatures. We use $M = 24, 32$, and 40 replicas.

A considerable challenge for the PT method is the selection of temperatures. As we are interested in globular states, thus we choose mostly low temperatures $T^* < T_\Theta^*$. For chains $(3-3)_{40}$ and $(6-6)_{20}$ we used $T_i^* \in [0.3; 1]$. For the $(10-10)_{12}$ chain we used $T_i^* \in [0.5; 1]$ because below 0.5 nothing seems to change in the polymer structure. However in each case for $\epsilon_{AB} \approx -\epsilon$ the highest value of T^* was 1.1 because coil-to-globule transition occurred for $T^* > 1$. The FOPT method is used to obtain an optimized temperature set. In this method we start with some temperature set (for example, linear or geometric) and run the simulation. In the next iteration we obtain a more optimal temperature set. A few iterations are required to obtain the optimized temperature set. This method is described in detail in Ref. 28 and it was applied to a polymer system in Ref. 29, and also in Ref. 30.

For each chain architecture we run five iterations of FOPT and we use the obtained temperature set in simulations. Each iteration of FOPT and each simulation consists of 5×10^5 MCS in athermal conditions (mixing) and at least 4×10^7 MCS in thermal conditions.

First 2×10^7 MCS are used to equilibrate system and the rest is used to collect data.

IV. RESULTS AND DISCUSSION

A. Chain with $(10-10)_{12}$ microarchitecture

First, we present the results for the $(10-10)_{12}$ multiblock chain with a compatibility parameter $\omega = 0.1$. At high temperatures this chain is in a coiled state, and it is expected to undergo the coil-to-globule transition upon cooling. Moreover, due to a low compatibility between A and B monomers, some ordered A- and B-rich nanostructures are also expected at low temperatures.

Indeed, the temperature dependencies for energy E^*/N, the heat capacity C_v, and the radius of gyration R_g^2 (in σ^2 units), shown in Fig. 1, indicate the above orderings as T^* is decreased. In particular, while E^*/N does not change much from high T^*'s to about $T^* \approx 1$, for smaller T^*'s it decreases rapidly, and this corresponds to a maximum in C_v, observed in Fig. 1(b). Also R_g^2 exhibits the most rapid change in this temperature region. Judging from the above and the position of the higher peak in C_v, we estimate the coil-to-globule transition temperature, as approximately $T^*_{CG} \approx 0.85$. We observe that below T^*_{CG}, R_g^2 is almost constant, decreasing slightly upon cooling. In Fig. 1(c) we can also observe a C_v maximum at about $T^* \approx 0.56$ and a "bump" in C_v at about $T^* \approx 0.75$. This is elucidated below in terms of the cluster formation.

Representative snapshots of the $(10-10)_{12}$ multiblock chain are shown in Fig. 2. A variety of globular structures can be seen, with the number of clusters decreasing upon cooling. This effect can be quantified by a cluster count distribution (CCD) diagram for different T^*, as shown in Fig. 3. As the system is cooled down to a globular state, the nanostructures with less clusters are more likely to be formed.

For $T^* \approx T^*_{CG}$ about 7- to 10-clusters are the most probable. The corresponding structures are loosely packed, disordered globules, as shown in in Fig. 2(b). At $T^* = 0.75$ the most probable structure is 4-cluster [Fig. 2(c)] with probability about 0.4, however tricluster [Fig. 2(d)] and 5-cluster are also very likely to be seen with probabilities of about 0.3 and 0.25, respectively. The remaining probability, 0.05, is distributed for the 6-cluster and dicluster structures. Then for $T^* = 0.62$ we observe a maximum in CCD for tricluster structures

with probability 0.9. This seems to correspond to the minimum in C_v for this T^*. Finally, at $T^* = 0.56$ we see that tricluster and dicluster [Fig. 2(e)] structures are equally probable with probability 0.5 (it corresponds to the second peak in C_v). At lower T^* we observe dicluster structures with probability approaching 1.

As noted above, for $T^* = 0.56$ we observe both a maximum in C_v and a transition from tricluster to dicluster structures in the CCD diagram. From this observation we suggest that the C_v bump for $T^* \approx 0.75$ is caused by structural changes from 6-cluster, through 5- and 4-cluster, to tricluster in this region.

Next, we simulate multiblocks with gradually higher compatibility parameters, from $\omega =$ 0.2 to 1.0. We show only representative CCD diagrams (Fig. 4). As we increase ω, the coil-to-globule transition occurs at gradually higher T^*'s. In Fig. 5 we show this transition for different ω's, and as it is increased, transformations between intra-globular structures with different number of clusters shift to higher T^*'s, in accordance with the T^*_{CG}'s behavior.

In Fig. 4(a) we show CCD for $\omega = 0.6$. For T^*'s between 0.6 and 0.7 probability of finding dicluster structures increase noticeably (compare with Fig. 3) and reaches about 0.3. For $\omega = 0.7$ [Fig. 4(b)] and the same T^* range, probabilities of finding dicluster and tricluster are almost equal. Further increasing of ω [Figs. 4(c) and 4(d)] causes higher probability of finding diclusters in this region with probabilities about 0.6 and 0.9 for $\omega = 0.8$ and 1.0, respectively.

This effect can be interpreted in terms of the site percolation problem [31]. For the highest compatibility $\omega = 1$, A and B monomers can freely mix, since energetically they are indistinguishable. In this case the copolymer chain becomes a homopolymer and the clusters have no physical meaning, but we analyze them formally in order to be consistent with the rest of this work. The effect described in this paragraph is also relevant to other ω's, but lower ω's, monomers are less miscible. At low T^*'s, the monomers are densely packed spheres in a globule and most of them have $Z = 12$ nearest neighbors. Since the type of two neighboring monomers is fixed (these are monomers along the chain - with an exception of the terminal monomers which have only one type of fixed neighbor), only $Z = 10$ neighbors of varied types. Critical percolation threshold for face centered cubic lattice (which can be used here since we have densely packed spheres in a globule) is $p_c \approx 0.119$ [31]. In our case, since we have 120 A and 120 B monomers, $p \approx 0.5$. Moreover in case of the $(10-10)_{12}$ chain there are always blocks of 10 monomers of the same type, therefore in this case it is

sufficient that only one of 10 monomers from the block has contact with another monomer of the same type in order to observe the percolation effect. Therefore the dicluster structures (in which each monomer type creates a continuous phase within globule) are very common.

For a better insight into dicluster structures we show representative snapshots of these structures at $T^* = 0.5$ (Fig. 6). As we increase ω from 0.1 to 0.5 the structural changes are small [compare Fig. 2(e) with 6(a)], then, as we increase it further, handshake structures prevail. In Fig. 6(b) we show a handshake structure and in Fig. 6(c) the same structure without B monomers. For $\omega = 0.9$ we find many handshake structures and tori with a core, where one type of monomers forms a torus around the other type [Fig. 6(d)]. Then for $\omega = 0.95$ we find more disordered structures, but very often monomers of the same type seem to aggregate [Fig. 6(e)]. Finally for $\omega = 1$ we observe disordered dicluster globules.

In Fig. 5 we show a phase diagram which collects data from all ω's for the $(10-10)_{12}$ chain. We want to stress that intra-globular structure is not exclusively defined by the number of clusters and that presented phase diagram shows regions with the most probable structures, but others are also present with smaller probabilities.

B. Structure factor

Since the CCD for a globule is not easily measurable experimentally, we calculate structure factor (measured in scattering experiments), $S(k)$, for the smallest compatibility $\omega = 0.1$. We select A-monomers as the scattering centers and calculate the isotropic $S(k)$ as follows:

$$S(k) = \frac{1}{N} \sum_{n,m} \frac{\sin k r_{nm}}{k r_{nm}} \tag{6}$$

where k is a scattering vector length and r_{nm} is a distance between monomer n and m. Results are presented in Fig. 7.

For all T^*'s we can observe a small maximum at $k \approx 0.94$, which corresponds to length of about 6.7σ. Since it is also visible for T^*'s above T^*_{CG} we can conclude that it corresponds to the extended size of a single block which is 10σ.

For $T^* = 0.7$ and 0.6 we can see another small maximum for $k \approx 1.7$ which corresponds to length 3.7σ. As we observe in Fig. 5, the most probable structure for those T^*'s is tricluster for which the thickness of the middle cluster of the globule is about 4σ. Therefore, we think

that this maximum is related to layers in the tricluster structures. This maximum is not visible for $T^* = 0.5$. In this temperature the most probable structure is dicluster and, since we "scatter" on A-monomers, we should obtain the structure factor of a flattened globule.

The above results indicate that the tricluster and dicluster structures may be distinguished experimentally by the $S(k)$ measurements.

C. Cluster count diagrams for other chain microarchitectures

The same procedure, as described above, is performed for $(6-6)_{20}$ and $(3-3)_{40}$ chains and results are presented in Fig. 8 and 9. In case of these chain microarchitectures it is necessary to simulate them at lower T^*'s than those for the $(10-10)_{12}$ chain, because many structural changes occur at lower temperatures.

First, we discuss results for the $(6-6)_{20}$ chain. The coil-to-globule transition occurs at a lower temperature, because the energy variations are smaller than those for the $(10-10)_{12}$ chain. This is related to a higher number of A-B contacts along the chain, and the fact that those contacts do not contribute effectively to the interaction energy.

In general, the regions of dominance for the 4-clusters and n-clusters (with $n > 4$) is similar to that for the $(10-10)_{12}$ chain, but it is different for di- and triclusters. We can see that tricluster structures for $\omega < 0.6$ are the most probable at low temperatures, whereas for previously discussed chain the dicluster structures prevail. This effect is explained in next section in terms of the interfacial surface minimization.

For $\omega > 0.6$ we observe a behavior similar to that of the $(10-10)_{12}$ chain. Monomers of different types mix and finally form disordered dicluster within globules, as explained earlier in terms of the site percolation problem.

Fig. 10 presents selected snapshots of structures observed for this chain. In Fig. 10(a) we see a tricluster for $\omega = 0.1$ with flat A-B interfaces. This structure dominates over wide range of ω's. However, as we increase ω's those tricluster structures become more spherical, for example, see Fig. 10(d) for $\omega = 0.7$, where the interfaces between A and B phases are more curved (like in handshake structures). For the same ω, but at higher T^*'s, dicluster structures dominate, exhibiting handshake structures, spiral structures [Figs. 10(b) and 10(c)] and others.

For $\omega \geq 0.8$ dicluster structures prevail in a wider T^*-range. Those dicluster structures

are very similar to those mentioned in previous paragraph. Also a torus with a core appears here [Figs. 10(f) and 10(g)].

Finally the $(3-3)_{40}$ microarchitecture is considered. The coil-to-globule transition occurs in lower T^*'s (Fig. 9), because there are more contacts between A and B monomers along the chain and therefore lower total energy.

Structures with a specified number of clusters occur in the same order as for the other chain architectures, but they appear at lower T^*'s. For $\omega \leq 0.3$ the most probable structures consists of 5 clusters arranged in layers [Figs. 11(a) and 11(b)]. For $\omega > 0.3$ at $T^* \approx 0.5$ we find 4-cluster structures and in lower T^* there is a region where 5-, 4-, and tricluster structures were almost equally probable and, in our simulations, we could not identify the dominating one. For $\omega > 0.4$ the tricluster structures dominate and for $\omega > 0.52$ dicluster structures dominate at low T^*'s. Again those dicluster structures are mixed A and B monomers and they appear for similar parameters (high ω and low T^*) as for the previously discussed chains.

Figure 11 presents snapshots of selected structures for the $(3-3)_{40}$ chain. We notice that increasing ω yields more curved structures, for example, the globule in Fig. 11(a) has a rather flat interfaces between A and B phases, but in Fig. 11(c) those interfaces are more curved. As they become more curved, they tend to connect with other layers. [see Figs. 11(d)-11(f)].

D. Types of observed structures

Structural changes observed in this work can be considered a result of the competition between two effects: minimization of the A-B interfacial area, that is the number of contacts between A and B, and minimization of the interfacial area between the chain and the solvent, that is the number of contacts between the chain and the solvent. Those effects are additionally influenced by the chain microarchitecture.

If we consider a mixture of spheres of two incompatible types, we will observe formation of two separate A- and B-rich phases. Adding bonds between spheres frustrates the phase separation and this system tries to find a structure, satisfying the chain microarchitecture constrains, with the minimum number of A-B contacts. For example, in symmetric diblock copolymer melts one can observe lamellar structures with flat A-B interfaces [3]. Asymmet-

ric diblock melts[32] or symmetric diblock melts with a solvent[3] form other nonlamellar structures, such as: gyroid, cylinders, and spheres.

On the other hand, in dilute polymer solutions, another minimization effect is also significant. Chains in a bad solvent minimize their contacts with solvent and form spherical globules, because sphere has the minimum surface area for a given volume. For block copolymer melts, a spherical confinement can be introduced artificially. As shown in Refs. 8 and 9 this confinement can yield structures similar to those presented in this study.

We assume, for the sake of this discussion, that the entropic effects are less significant, and are not addressed. The observed structures are thought to be a result of a delicate interplay between the two above enthalpic effects. Varying ω's changes the relative contributions of those two effects. Increasing ω makes the first effect less significant. In the limit, $\omega = 1$, the first effect disappears (since A and B monomers are fully miscible). From snapshots presented in this work, it can be seen that for chains with higher ω's globules are more spherical than those with lower ω's.

As an example, we consider formation of tricluster structures in $(6-6)_{20}$ chain for $\omega = 0.1$ at $T^* < 0.58$. Figure 10(a) presents snapshot of a globule for those parameters. It is a tricluster structure with clusters arranged in layers with almost flat A-B interfaces. This globule has an elliptical shape. Dicluster with a flat A-B interface seem to provide the smallest possible interfacial area, but to keep it flat, a globule as a whole must be considerably flattened, what increases the contacts between chain and solvent. On the other hand, compacting it into more spherical shape increases the A-B interface curvature. As a result one type of monomers forms two separate clusters which order lamellarly. Increasing ω results in forming more spherical globules and therefore in increasing interface area between different types of monomers (see Fig. 10), since, as described earlier, the A-B penalty for contacts is smaller for higher ω's.

Within-globular orderings can be related to the nanophase separations in block copolymers, because a globule is locally dense system. Since only symmetric block sizes were used in this work, structures should correspond to bulk symmetric diblock copolymers. In such systems lamellar phases are expected (however gyroid, perforated lamellae, cylinders, and other structures were recently found in sulfonated diblock copolymers with symmetric block sizes both in experiment [33] and in simulation [34]). Changing the A-B interaction potentials should only shift the order-disorder transitions temperature and it should not easily lead

to formation of nonlamellar structures. Why, therefore, we observe handshake, spiral, and other nonlamellar configurations? As indicated earlier, we consider it a result of a delicate interplay of two effects. As we increase compatibility, the minimization of contacts between chain and solvent becomes a stronger effect than the minimization of the A-B interfacial area, and in order to form more spherical shapes of a globule, the A-B interfaces tend to be more curved. Thus, as a result we obtain the handshake, spiral, and other structures.

We conjecture that asymmetric block sizes are necessary to obtain gyroid-like structures within a single globule. However they were not considered in this work. Probing different microarchitectures may lead to many other structures, for example sufficiently long chains should reproduce a richer phase diagram with a cylindrical, gyroidal, or spherical intra-globular structures.

E. Intra-globular structures and native states of proteins

This coarse-grained model is probably too simplified to capture the complexity of protein behavior, but it still may shed some light on it. For example, in order to create helical structures, hydrogen bonds are necessary [13]. Therefore, the spiral structures observed in this study are not a manifestation of the helical-like structures found in polypeptide chains, because our spirals are relatively thick–of the order of few monomers in diameter [see Fig. 10(c)].

Amino acids can be roughly divided into two groups: hydrophobic and polar. Most of simplified coarse-grained protein models capture mainly this property. However, in our model solvent is nonselective and it becomes poor when we decrease T^*. Therefore we can consider those globules as a hydrophobic cores consisting of two types of amino acids.

In this work we do not observe a single native state. As can be seen in CCD diagrams (Figs. 3 and 4) for a given T^*, structures with different number of clusters can coexist. Only for the lowest T^*'s probability of finding structures with a given number of clusters approaches 1. But even in such case, there is degeneration of "native" states, because in order to obtain it, chain can be folded in a variety of ways. For example, in order to form dicluster structure like in Fig. 6(a) it does not matter where different A blocks are, as long as they are inside the A cluster.

However we would like to emphasize that the low compatibility between monomers re-

duces the degeneracy of the inter-globular structures. There are less possible ways to fold a chain into lamellar-like structure than into a disordered globule.

V. CONCLUSION

We present an extensive Monte Carlo study of intra-globular structures of long multiblock copolymer chains with alternating blocks, using a discontinuous interaction potential.

Due to the chain architecture constrains, the interplay of minimization of the A-B interface with the minimization of the polymer-solvent interface yields a rich phase diagram with a variety of intra-globular structures, such as handshake, spiral, tricluster, torus with a core, lamellar, and many other mixed and disordered structures. We relate our results to those for block copolymer nanophases in bulk, and find many similarities between them, especially in spherical confinement. We also expect that other intra-globular structures may be present in multiblock copolymer chains with asymmetric blocks, such as analogs of gyroidal, cylindrical and spherical nanophases.

We analyzed the $(10-10)_{12}$ chain behavior for various T^*'s and ω's. From this analysis, and similar analysis of other chains [$(6-6)_{20}$ and $(10-10)_{12}$], we construct phase diagrams in (T^*,ω)-space of the most probable n-cluster structures. In each case decreasing T^* leads to coil-to-globule transition, followed by transitions between structures with n-clusters (n decreases with T^*). The smallest n for low ω and low T^* was 2, 3 and 5 for $(10-10)_{12}$, $(6-6)_{20}$, and $(3-3)_{40}$, respectively.

From the structure factor of $(10-10)_{12}$ chain we can distinguish tricluster and dicluster structures, and therefore it is possible to relate the numerical predictions to an experiment.

Finally, we show that despite of the simplicity of this model, it still may shed some light on highly complex behavior of proteins, for example: varying compatibility between monomers within hydrophobic core may reduce of the degeneracy of the ground states.

ACKNOWLEDGMENTS

We gratefully acknowledge the computational grant from the Poznan Supercomputing and Networking Center (PCSS) and grant N202 287338 from Polish Ministry of Science and Higher Education.

[1] D. F. Parsons and D. R. M. Williams, Phys. Rev. Lett. **99**, 228302 (2007).

[2] I. W. Hamley, *Developments in Block Copolymer Science and Technology* (John Wiley & Sons, Berlin, 2004).

[3] S. Wołoszczuk, M. Banaszak, P. Knychała, and M. Radosz, Macromolecules **41**, 5945 (2008).

[4] P. Cheolmin, Y. Jongseung, and L. T. Edwin, Polymer **44**, 6725 (2003).

[5] W. Li, R. A. Wickham, and R. A. Garbary, Macromolecules **39**, 806 (2006).

[6] X. He, M. Song, H. Liang, and C. Pan, J. Chem. Phys. **114**, 10510 (2001).

[7] B. Yu, P. Sun, T. Chen, Q. Jin, D. Ding, B. Li, and A. . Shi, J. Chem. Phys. **126** (2007).

[8] B. Yu, B. Li, Q. Jin, D. Ding, and A. . Shi, Macromolecules **40**, 9133 (2007).

[9] S. Piotto, S. Concilio, F. Mavelli, and P. Iannelli, Macromol. Symp. **286**, 25 (2009).

[10] S. Schnabel, M. Bachmann, and W. Janke, J. Chem. Phys. **131**, 124904 (2009).

[11] S. Schnabel, T. Vogel, M. Bachmann, and W. Janke, Chem. Phys. Lett. **476**, 201 (2009).

[12] D. T. Seaton, T. Wüst, and D. P. Landau, Phys. Rev. E **81**, 1 (2010).

[13] E. Shakhnovich, Chem. Rev. **106**, 1559 (2006).

[14] Y. S. Djikaev and E. Ruckenstein, Adv. Colloid Interface **146**, 18 (2009).

[15] J. Schluttig, M. Bachmann, and W. Janke, J. Comp. Chem. **29** (2008).

[16] J. N. Onuchic, P. G. Wolynes, Z. Luthey-Schulten, and N. D. Socci, Proc. Natl. Acad. Sci. U.S.A. **92**, 3626 (1995).

[17] K. Yue, K. M. Fiebig, P. D. Thomas, H. S. Chan, E. I. Shakhnovich, and K. A. Dill, Proc. Natl. Acad. Sci. U.S.A. **92**, 325 (1995).

[18] R. Schiemann, M. Bachmann, and W. Janke, J. Chem. Phys. **122**, 114705 (2005).

[19] J. Straub and D. Thirumalai, Proc. Nad. Acad. Sci. USA **90**, 809 (1993).

[20] S. Miyazawa and R. L. Jernigan, J. Mol. Biol. **256**, 623 (1996).

[21] E. I. Shakhnovich, Phys. Rev. Lett. **72**, 3907 (1994).

[22] Y. Zhou, C. Hall, and M. Karplus, Phys. Rev. Lett. **77**, 2822 (1996).

[23] K. Lewandowski, P. Knychała, and M. Banaszak, Phys. Status Solidi B **245**, 2524 (2008).

[24] S. Wołoszczuk, M. Banaszak, P. Knychała, K. Lewandowski, and M. Radosz, J. Non-Cryst. Solids **354**, 4138 (2008).

[25] K. Lewandowski and M. Banaszak, J. Non-Cryst. Solids **355**, 1289 (2009).

[26] N. Metropolis, A. Rosenbluth, M. Rosenbluth, and A. Teller, J. Chem. Phys. **21**, 1087 (1953).

[27] D. J. Earl and M. W. Deem, Phys. Chem. Chem. Phys. **7**, 3910 (2005).

[28] H. G. Katzgraber, S. Trebst, D. A. Huse, and M. Troyer, J. Stat. Mech. , P03018 (2006).

[29] K. Lewandowski, P. Knychała, and M. Banaszak, CMST **16(1)**, 29 (2010).

[30] T. Beardsley and M. Matsen, Eur. Phys. J. E **32**, 255 (2010).

[31] M. Sykes, D. Gaunt, and M. Glen, J. Phys. A: Math. Gen. **9**, 1705 (1976).

[32] M. Matsen, G. Griffiths, R. Wickham, and O. Vassiliew, J. Chem. Phys. **124**, 024904 (2006).

[33] M. J. Park and N. P. Balsara, Macromolecules **41**, 3678 (2008).

[34] P. Knychała, M. Banaszak, M. J. Park, and N. P. Balsara, Macromolecules **42**, 8925 (2009).

FIGURE CAPTIONS

Fig. 1: Results for the $(10-10)_{12}$ chain (error bars are also shown): (a) reduced energy per monomer E^*/N, as a function of reduced temperature T^*; (b) specific heat, C_v, as a function of T^*; (c) squared radius of gyration, R_g^2, as a function of T^*.

Fig. 2: (Color online) Representative snapshots of the $(10-10)_{12}$ chain with compatibility $\omega = 0.1$ in different temperatures: (a) swollen state at $T^* = 1.2$, (b) coil-to-globule transition at $T^*_{CG} = 0.85$, (c) 4-cluster structure at $T^* = 0.75$, (d) tricluster structure at $T^* = 0.62$ and (e) dicluster structure at $T^* = 0.5$.

Fig. 3: Probability of finding n-cluster structure p_n, as a function of reduced temperature T^*, for the $(10-10)_{12}$ chain with compatibility $\omega = 0.1$. For clarity, only selected p_n lines are shown.

Fig. 4: Probability of finding n-cluster structure p_n, as a function of reduced temperature T^*, for the $(10-10)_{12}$ chain with compatibility: (a) $\omega = 0.6$, (b) $\omega = 0.7$, (c) $\omega = 0.8$, and (d) $\omega = 1.0$. For clarity, only selected p_n lines are shown.

Fig. 5: Phase diagram for the $(10-10)_{12}$ chain in (T^*, ω)-space. Dashed line shows coil-globule transition. Solid lines divides regions with the greatest probability of finding n-cluster structures. Many-cluster region consists of structures with $n > 5$ clusters.

Fig. 6: (Color online) Variety of dicluster structures for the $(10-10)_{12}$ chain at $T^* = 0.5$ for compatibility: (a) $\omega = 0.5$, (b) $\omega = 0.8$, (c) $\omega = 0.8$ (without B monomers), (d) $\omega = 0.9$, (e) $\omega = 0.95$, and (f) $\omega = 1$.

Fig. 7: Structure factor $S(k)$ for the $(10-10)_{12}$ chain with $\omega = 0.1$ at $T^* = 1.4$, 0.9, 0.8, 0.7, 0.6, and 0.5. The scattering profiles are offset vertically by factors of 10, 10^2, 10^3, 10^4, and 10^5, for clarity.

Fig. 8: Phase diagram for the $(6-6)_{20}$ chain in (T^*, ω)-space. Dashed line shows coil-globule transition. Solid lines divides regions with the greatest probability of finding n-cluster structures. Many-cluster region consists of structures with $n > 5$ clusters.

Fig. 9: Phase diagram for the $(3-3)_{40}$ chain in (T^*, ω)-space. Dashed line shows coil-globule transition. Solid lines divides regions with the greatest probability of finding n-cluster structures. Many-cluster region consists of structures with $n > 5$ clusters. In 5/4/3 region probabilities of finding 5-, 4-, and triclusters is almost equal.

Fig 10: (Color online) Variety of structures for the $(6-6)_{20}$ chain at $T^* = 0.3$ for compatibility: (a) $\omega = 0.1$ (tricluster), (b) $\omega = 0.7$ (at $T^* = 0.5$, dicluster), (c) $\omega = 0.7$ (at

$T^* = 0.5$, without B monomers, dicluster), (d) $\omega = 0.7$ (tricluster), (e) $\omega = 0.9$ (dicluster), (f) $\omega = 0.8$ (dicluster), (g) $\omega = 0.8$ (without B monomers, dicluster).

Fig. 11: (Color online) Variety of structures for the $(3-3)_{40}$ chain at $T^* = 0.3$ for compatibility: (a) $\omega = 0.1$ (5-cluster, lamellar), (b) $\omega = 0.1$ (without B monomers, 5-cluster, lamellar), (c) $\omega = 0.31$ (4-cluster, lamellar), (d) $\omega = 0.5$ (at $T^* = 0.5$, tricluster),)e) $\omega = 0.51$ (tricluster), (f) $\omega = 0.51$ (without B monomers, tricluster).

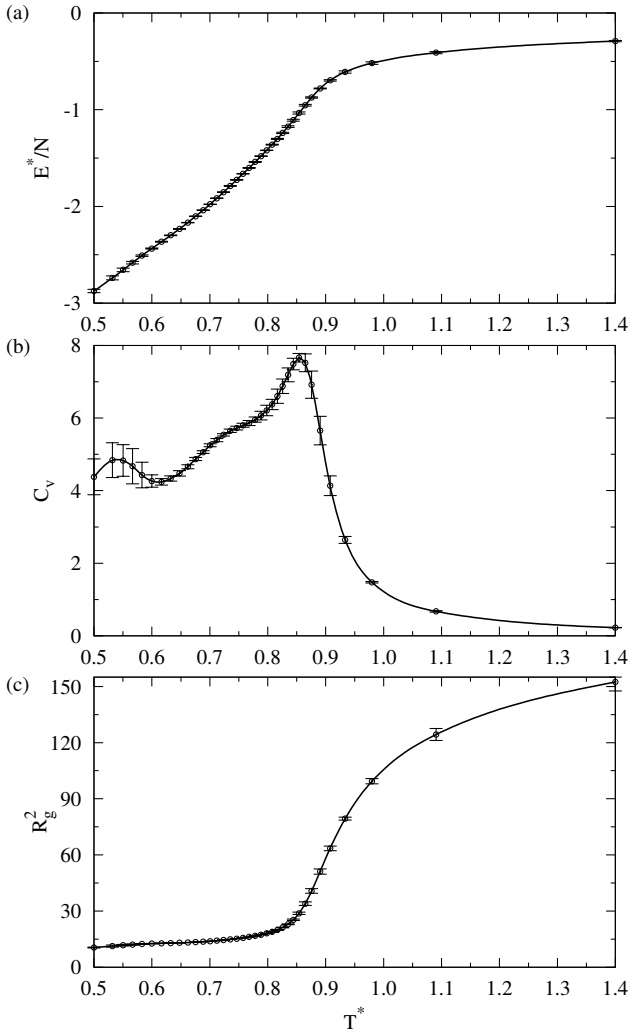

FIG. 1. Lewandowski and Banaszak

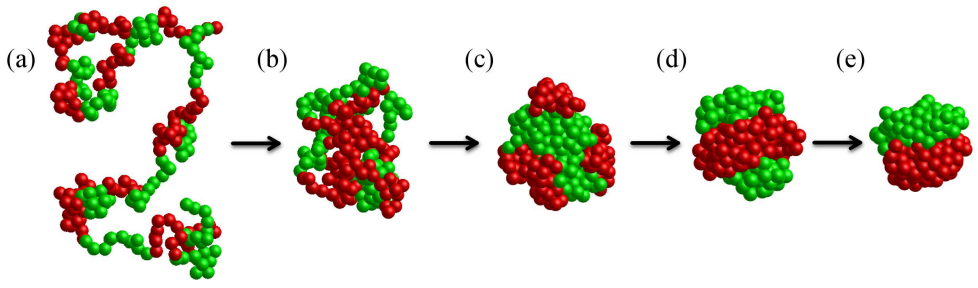

FIG. 2. Lewandowski and Banaszak

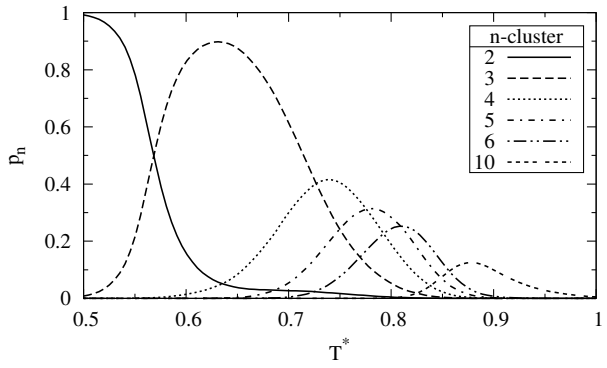

FIG. 3. Lewandowski and Banaszak

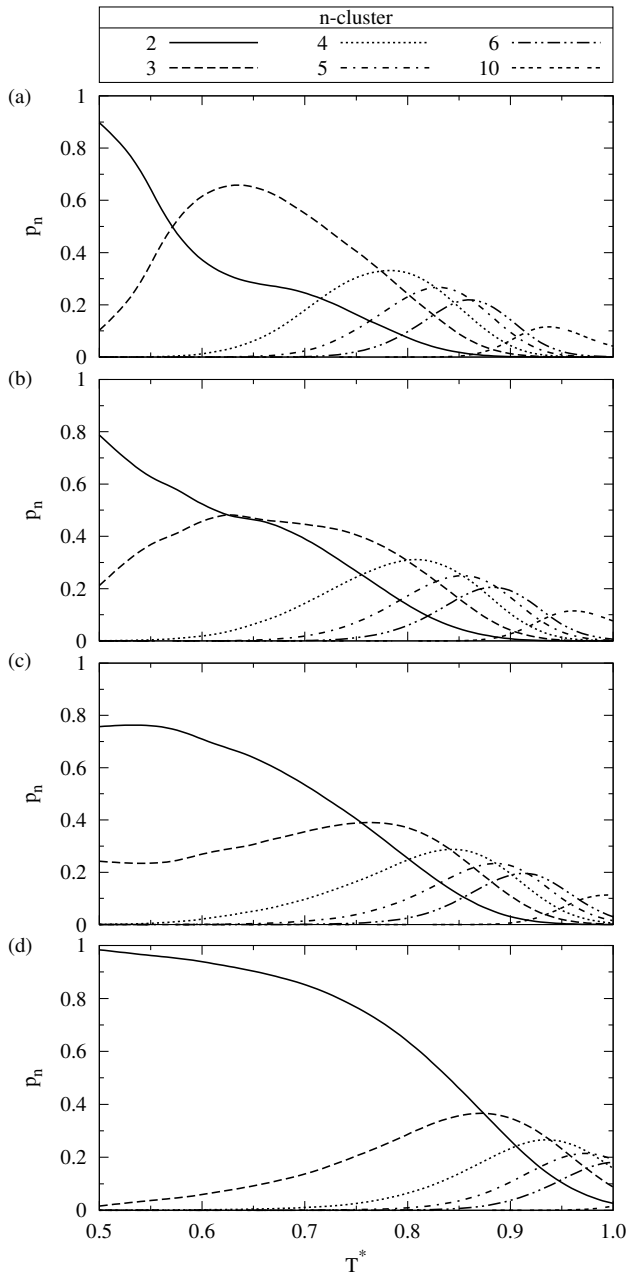

FIG. 4. Lewandowski and Banaszak

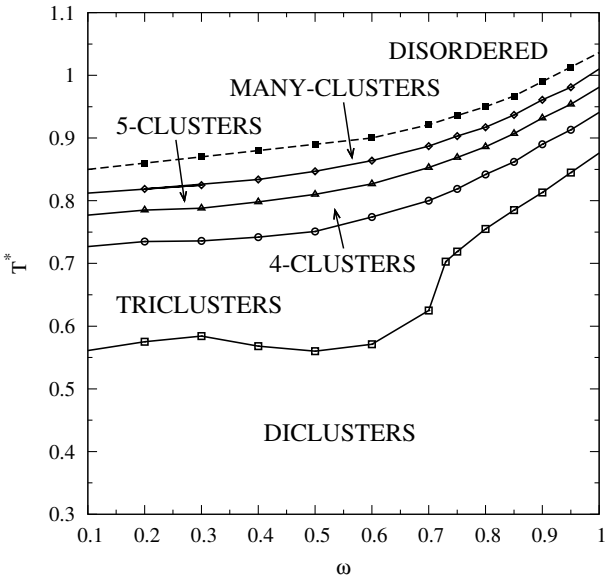

FIG. 5. Lewandowski and Banaszak

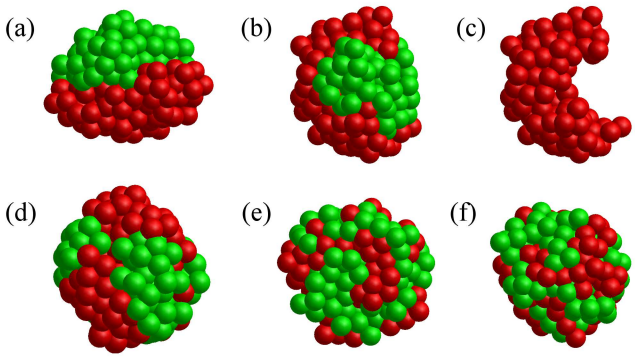

FIG. 6. Lewandowski and Banaszak

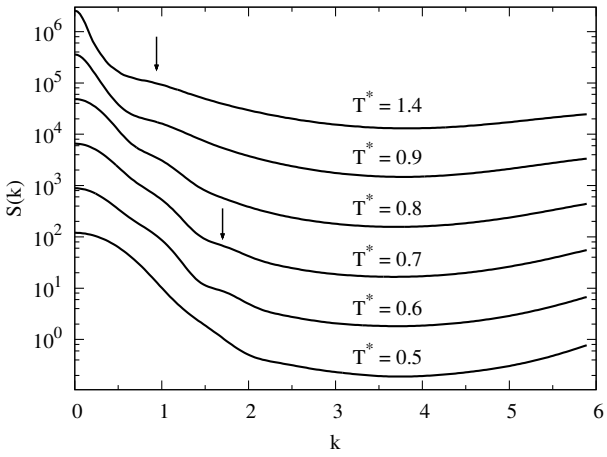

FIG. 7. Lewandowski and Banaszak

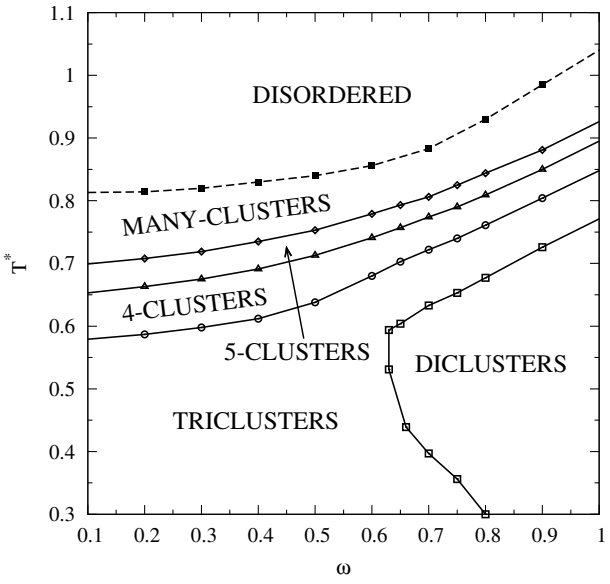

FIG. 8. Lewandowski and Banaszak

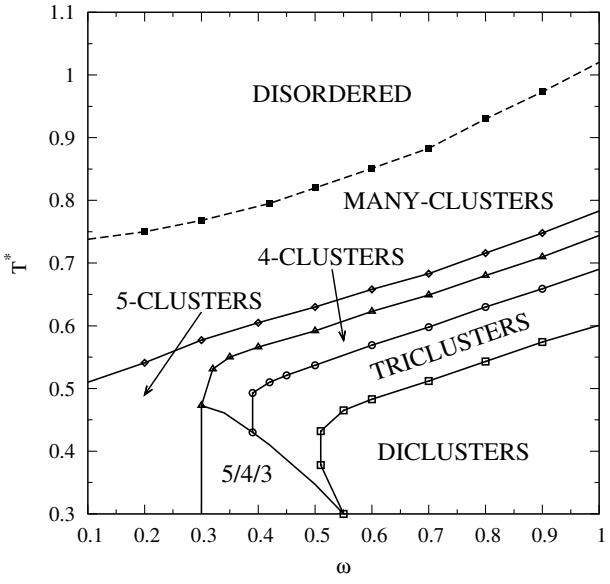

FIG. 9. Lewandowski and Banaszak

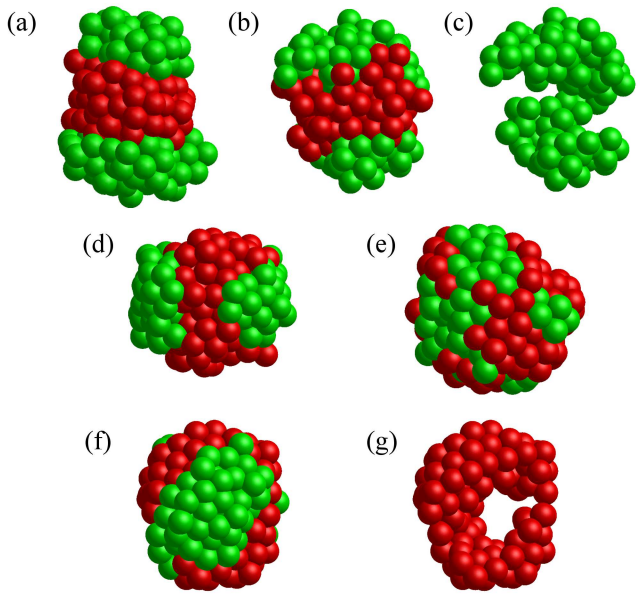

FIG. 10. Lewandowski and Banaszak

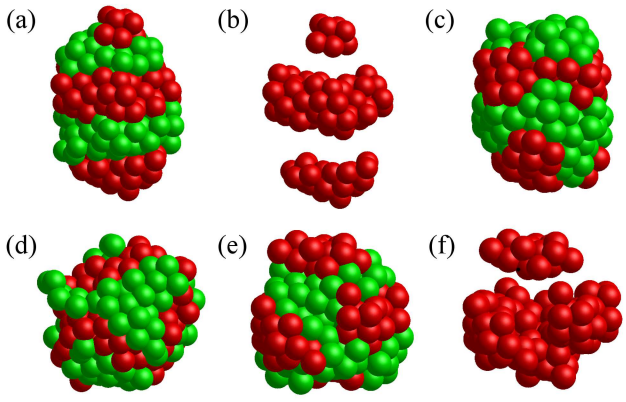

FIG. 11. Lewandowski and Banaszak